01 Nov 2001

Electron-Impact Excitation to the $4p^5 5s$ and $4p^5 5p$ Levels of Kr | Using Different Distorted-Wave and Close-Coupling Methods

Arati K. Dasgupta

Klaus Bartschat

D. Vaid

Alexei N. Grum-Grzhimailo

et. al. For a complete list of authors, see https://scholarsmine.mst.edu/phys_facwork/1527

Recommended Citation

A. K. Dasgupta et al., "Electron-Impact Excitation to the $4p^5 5s$ and $4p^5 5p$ Levels of Kr | Using Different Distorted-Wave and Close-Coupling Methods," *Physical Review A. Atomic, Molecular, and Optical Physics*, vol. 64, no. 5, pp. 052710-1-052710-10, American Institute of Physics (AIP), Nov 2001.
The definitive version is available at https://doi.org/10.1103/PhysRevA.64.052710

Electron-impact excitation to the $4p^5 5s$ and $4p^5 5p$ levels of Kr I using different distorted-wave and close-coupling methods

A. Dasgupta,[1] K. Bartschat,[2] D. Vaid,[3] A. N. Grum-Grzhimailo,[4] D. H. Madison,[3] M. Blaha,[5] and J. L. Giuliani[1]
[1]*Radiation Hydrodynamics Branch, Plasma Physics Division, Naval Research Laboratory, Washington, District of Columbia 20375*
[2]*Department of Physics and Astronomy, Drake University, Des Moines, Iowa 50311*
[3]*Physics Department, University of Missouri-Rolla, Rolla, Missouri 65401*
[4]*Institute of Nuclear Physics, Moscow State University, 119899 Moscow, Russia*
[5]*6716 Lamont Drive, Lanham, Maryland 20706*
(Received 26 April 2001; published 5 October 2001)

Electron-impact excitation of the $4p^5 5s$ and $4p^5 5p$ levels of Kr I has been investigated in detail by calculating cross sections using distorted-wave and close-coupling approaches. The results are presented from the excitation thresholds up to 50 eV incident energy. They are contrasted among the different calculations and compared with other theoretical predictions and experimental data. Significant disagreement is found with many of the recent experimental data of Chilton *et al.* [Phys. Rev. A **62**, 032714 (2000)].

DOI: 10.1103/PhysRevA.64.052710 PACS number(s): 34.80.Dp

I. INTRODUCTION

Electron-impact excitation of rare gases such as argon and krypton has received considerable interest due to the importance of these noble gases in many gaseous electronic applications. These gases are heavily used in plasma processing of flat-panel displays and semiconductor manufacturing, lighting industries, gas-discharge lamps [1], and in gas lasers. In multispecies actinometry, both argon and krypton are used as seed gases to determine the dissociation fraction of a molecular gas, such as nitrogen, by comparing the emission lines from these rare gases and the gas of interest. An accurate knowledge of the excitation cross sections is crucial for this determination of the dissociation fraction and the diagnostics of plasma conditions of the atomic-species involved [2,3]. In addition to the need for low-energy excitation cross sections in most of these applications, high-energy excitation as well as ionization cross sections are important in KrF gas-laser systems where the amplifier cells are pumped by a high-energetic electron beam. One thus needs the cross sections over a wide range of projectile energies. Growing need for excitation cross sections of neutral rare gases in industrial applications, as well as for a better understanding of fundamental atomic-collision physics, have resulted in many-recent theoretical and experimental investigations. Several calculations and the corresponding data sets have been published and made generally available for electron-impact excitations of Ar I (see recent publications [4–7] and references therein), but similar investigations of Kr I are very limited.

Most of the published work to date has concentrated on elastic and inelastic cross sections to the lowest four $4p^5 5s$ levels of Kr I [8,9], with much attention devoted to the resonance structure due to compound states near the excitation thresholds (see [10,11] and references therein). Calculated integral cross sections to the $4p^5 5p$ levels obtained in the relativistic distorted-wave approximation were reported by Kaur *et al.* [12], but not all transitions in the multiplet were considered and the results for separate levels were not discussed. On the experimental side, there exist energy-loss measurements of total cross sections by Trajmar *et al.* [9]. Because of their limited energy resolution, however, these authors combined the cross sections to several of the closely lying $5p$ levels. Also, extrapolation of the differential cross sections results in additional uncertainties beyond those for direct measurements of integral cross sections. Much better resolution is achieved by the optical method, where all states of the $4p^5 5p$ configuration are easily resolved. Measurements of the optical-excitation functions for the $4p^5 5p$ states in Kr excited by electron impact were done a long-time ago [13,14], but a careful analysis of the corresponding data is needed to accurately subtract the cascade cross sections and to avoid pressure effects in order to obtain the direct excitation cross sections. Bogdanova and Yurgenson [15], using the optical method in a combination with a pulsed electron beam to suppress secondary processes populating the excited levels, reported direct-excitation cross sections to the $5p$ levels only for two high electron energies (100 eV and 200 eV) and the peak cross-section values. Very recently, the Wisconsin group [16] systematically measured the total-direct excitation cross sections to all ten $4p^5 5p$ levels by using the optical method with careful analysis of cascading and pressure effects. To the best of our knowledge, no detailed theoretical calculations have been published to date for all of these levels. Also, even among the reported theoretical and experimental investigations, one sometimes finds vast differences among the results. This fact, together with the need for an accurate determination of these cross sections to support the various model applications mentioned above, necessitates systematic studies of these quantities. In this work, we therefore present detailed calculations of the angle-integrated cross sections to all-four levels of the $4p^5 5s$ configuration and to the ten $4p^5 5p$ levels of Kr I for excitation from the ground state $4p^6\ {}^1S_0$.

We have calculated the angle-integrated cross sections to the 14 levels using three-different theoretical approaches. They are the semirelativistic distorted-wave method developed by Dasgupta, Blaha, and Giuliani [7] (to be referred to as DW-1 below), which explicitly includes a long-range po-

larization potential, the semirelativistic first-order distorted-wave approximation of Madison and Shelton [17] (to be labeled as DW-2), used extensively by Bartschat and Madison [18], and the semirelativistic Breit-Pauli *R*-matrix (BPRM) approach of the Belfast group [19]. The latter method applies a close-coupling-type model and was used by Bartschat and collaborators [5,20–23] to treat electron-impact excitation of heavy noble gases.

Since the nonperturbative BPRM method couples the various open and closed channels, it is generally expected to predict better results near the excitation thresholds compared to the perturbative distorted-wave methods, particularly, if resonance effects are important. As the energy increases, however, channel coupling becomes less important and *R*-matrix approaches, in particular, may face convergence problems due to the large number of basis functions that are needed to represent the continuum electron in the various channels. In addition, the standard Belfast *R*-matrix code, like most other close-coupling programs, requires the use of a common set of orthogonal one-electron orbitals to represent all the states in the coupled-channel expansion. Consequently, it is often necessary to compromise on the quality of the target description, i.e., it is computationally prohibitive to use a target description that has been optimized to represent the initial and final states of a particular transition as well as possible.

The less-complex distorted-wave methods are, therefore, often more suitable to treat higher-electron energies. Due to the smooth energy dependence of the cross sections, the calculation only needs to be performed for a relatively small number of incident energies. Furthermore, it is generally easy to include as many partial waves as needed for convergence, especially since the ''top up'' to the plane-wave Born approximation is straightforward. In addition, physical effects that would be included *ab initio* in an all-electron close-coupling model, such as exchange with the core, the polarization of the target charge cloud due to the projectile, and even absorption into channels other than the final state of interest, can be simulated by applying properly constructed pseudopotentials (see, for example, Ref. [18]).

Consequently, one would expect that the two perturbative (DW) and nonperturbative (RM) methods can complement each other to cover a wide range of incident energies. Indeed, this was demonstrated successfully by Maloney *et al.* [6]. The motivation behind the present work was thus to examine the differences in the results obtained in the above approaches and to compare the results with experimental data. Ultimately, this should allow us to decide to what extent the difficult problem of electron-impact excitation of a heavy noble gas such as krypton can be treated efficiently by employing a combination of the most promising methods for the respective energy ranges, in which one expects their fundamental assumptions to be valid. The by-product of such work should be a set of the most reliable collision cross sections currently available for modeling applications.

In Sec. II, we briefly describe the different theoretical methods and indicate some of the relevant computational details applied in this work. Our results are presented in Sec. III and compared among themselves, with other theoretical predictions, and also with experimental data. Finally, the conclusions are summarized in Sec. IV. Unless otherwise indicated, atomic units are used throughout this manuscript.

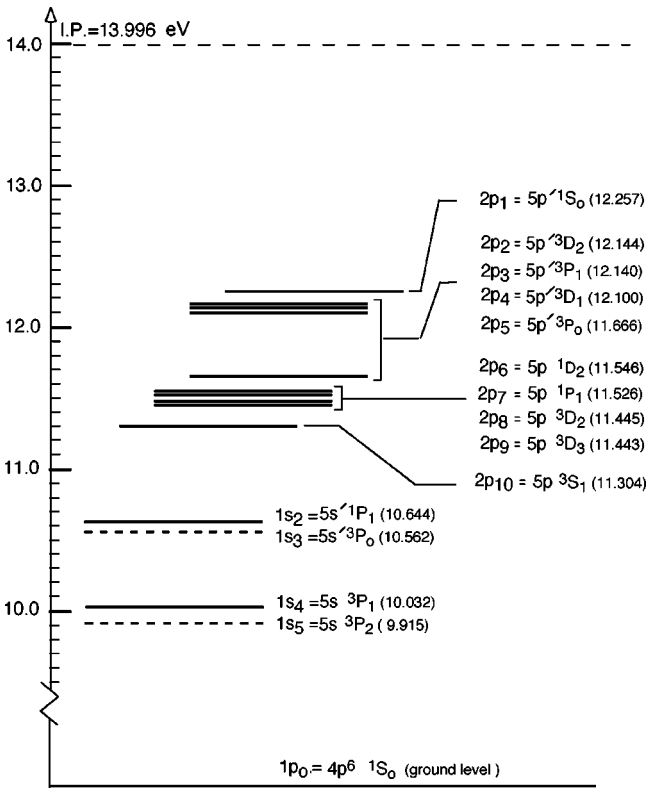

FIG. 1. Energy-level diagram showing the $4p^5 5s$ ($1s_5$-$1s_2$) and $4p^5 5p$ ($2p_{10}$-$2p_1$) levels of Kr I. The dashed lines show the two-metastable levels $1s_5$ and $1s_3$.

II. COMPUTATIONAL METHODS

Figure 1 shows an energy-level diagram of Kr I, with the experimental energies given by Moore [24]. The figure only includes the ground state and the 14 relevant excited $4p^5 5s$ and $4p^5 5p$ levels. Both the Racah and the Paschen notations ($1p_0$ for the ground state, $1s_5$-$1s_2$ for $4p^5 5s$, and $2p_{10}$-$2p_1$ for the $4p^5 5p$ configuration) are indicated. This energy-level structure is very similar to that of Ar I [16,7], but the energy gap between levels associated with the $^2P_{3/2}$ ($2p_{10}$-$2p_5$) and the $^2P_{1/2}$ ($2p_4$-$2p_1$) doublet of the $4p^5$ core is significantly larger in Kr I than it is in Ar I.

A. DW-1 method

We have used the basic method described in detail in [7], but the following important modifications should be mentioned. In the present calculation, we have included relativistic corrections explicitly in optimizing the bound-state wave functions by including the mass-velocity and the Darwin terms in the distorting potential while the spin-orbit interaction was included by diagonalizing the atomic Hamiltonian for mixing among levels with the same total electronic angular momentum J as described in [7].

The valence orbital P_{nl} was generated by solving the differential equation

$$\left[\frac{d^2}{dr^2}-\frac{l(l+1)}{r^2}-2\{V_0(r)+\beta V_{ex}(r)+V_p(r)+V_D(r)+V_{mv}(r)-E_{nl}\}\right]P_{nl}(r)=-\sum_{n'<n}\mu_{n'l}P_{n'l}(r). \quad (1)$$

Here $V_0(r)$ and $V_{ex}(r)$ are the Coulomb and the static-exchange potentials of the ionic core, and the parameter β was varied to obtain the experimental binding energy E_{nl} for the fine-structure level of interest. The sum on the right-hand side of Eq. (1), involving the Lagrange multipliers $\mu_{n'l}$, ensures that P_{nl} is orthogonal to the other bound orbitals with the same angular momentum l. Finally, $V_D(r)$ and $V_{mv}(r)$ are the relativistic Darwin and mass-velocity terms while $V_p(r)$ is a polarization potential. For small radii, $r \leqslant r_c$, we adopted the correlation polarization potential $V_p[\rho(r)]$, first introduced by O'Connell and Lane [25], with the analytic form

$$\begin{aligned} V_p(r_s) &= 0.0622\ln r_s - 0.096 + 0.018 r_s \ln r_s - 0.02 r_s, \\ & \quad r_s \leqslant 0.7 \\ &= -0.1231 + 0.03796 \ln r_s, \quad 0.7 \leqslant r_s \leqslant 10 \\ &= -0.876 r_s^{-1} + 2.65 r_s^{-3/2} - 2.8 r_s^{-2} - 0.8 r_s^{-5/2}, \\ & \quad 10 \leqslant r_s \leqslant r_c. \end{aligned} \quad (2)$$

Here $r_s=[3/4\pi\rho(r)]^{1/3}$, with $\rho(r)$ denoting the charge density, and r_c is the first crossing point of the above potential with the long-range form given by $V_p(r)=-\alpha_d/2r^4$. The dipole polarizability α_d was taken as $16.8a_0^3$ [26]. Finally, the $1s$, $2s$, $2p$, $3s$, $3p$, $3d$, and $4s$ orbitals were generated by using the parameters given by Clementi and Roetti [27].

The radial parts of the distorted waves were obtained by solving an equation similar to Eq. (1), except that V_0 now represented the static potential of the neutral target and E_{nl} was replaced by the positive energy of the free electron. Also, the weight of the exchange potential V_{ex} was not varied ($\beta \equiv 1$) and the relativistic terms V_D and V_{mv} were no longer included. The final-state interaction was used for both the entrance and the exit channel in calculating the distorted waves, as this procedure is expected to give the best overall results [28].

The elements of the reactance matrix **K** were calculated using the known asymptotic form of the collision wave function. Using these results, the transition matrix **T** and the scattering matrix **S** were obtained from the relations

$$\mathbf{S}=1+\mathbf{T}=\frac{(1+i\mathbf{K})}{(1-i\mathbf{K})}. \quad (3)$$

It is worth pointing out that the **S** matrix, if calculated directly from the first-order perturbation theory employed in this method, may not be unitary. On the other hand, if the **K** matrix is calculated first using an approximate method, then the **S** matrix obtained from Eq. (3) is unitary. It is this unitarization of the **S** matrix that guarantees the conservation of flux from the incoming and outgoing beams, and this may become very important, particularly near threshold (see below).

The collision cross sections $Q(\alpha SLJ,\alpha' S' L' J')$ for fine-structure transitions $\alpha SLJ \rightarrow \alpha' S' L' J'$ were expressed in terms of the transition-matrix elements $T(\alpha SL,\alpha' S' L')$. As indicated, these elements were first calculated in the nonrelativistic LS scheme. Then they were transformed to an intermediate coupling scheme, and the relationship

$$Q(\alpha SLJ,\alpha' S' L' J')=\frac{\pi k^{-2}}{2(2J+1)}\sum_{ll'jj'J_T}(2J_T+1)\times|T(\alpha SLJljJ_T;\alpha' S' L' J' l' j' J_T)|^2 \quad (4)$$

was used. Here J_T is the electronic angular momentum of the combined system, target plus projectile, coupled from the individual angular momenta J and j, respectively.

Using the unitarization method described above, we assumed that the spin-orbit coupling of atomic electrons is weak during the collision, i.e., the atom behaves as if it were temporarily in pure LS states that only need to be recoupled to form SLJ states after the collision. For more details, including a form of unitarization where the **K**-matrix elements are transformed first, we refer to the paper by Dasgupta *et al.* [7].

B. DW-2 method

The second distorted-wave approach we have used, to be labeled as DW-2, is the semirelativistic first-order distorted-wave approximation of Madison and Shelton (1973) and of Bartschat and Madison (1987). Since the details of the theory may be found in the above references, only a brief outline is presented here. In contrast to the DW-1 approach, where the atomic wave functions were calculated separately for each final state and optimized for that state, the atomic wave functions used in the DW-2 approach were the same as those in the 15-state R-matrix calculation described below. While this choice has the advantage of providing a consistent set of wave functions for all states of interest, it has the disadvantage of not being the best possible representation for any particular final state.

The second difference between the DW-1 and DW-2 methods lies in the fact that relativistic effects are included in the calculation of the continuum distorted waves for DW-2. For DW-2, each of the radial distorted waves is a solution of Schrödinger's equation including relativistic effects:

$$\left[\frac{d^2}{dr^2}-\frac{l(l+1)}{r^2}-2\{U(r)+V_r(r)-E\}\right]\chi_l(r)=0. \quad (5)$$

Here $U(r)$ is the static Coulomb potential plus the static exchange potential, i.e.,

$$U(r)=V_0(r)+V_{ex}(r), \quad (6)$$

and $V_r(r)$ contains the relativistic effects

$$2V_r = 2\gamma U(r) - [\alpha U(r)]^2 - \frac{(j+1)}{r}\frac{\eta(r)'}{\eta(r)} + \frac{3}{4}\left[\frac{\eta(r)'}{\eta(r)}\right]^2 - \frac{1}{2}\frac{\eta(r)''}{\eta(r)}, \quad (7)$$

where

$$\gamma = \sqrt{1+2\alpha^2 E} \quad (8)$$

and

$$\eta(r) = 1 + \gamma - \alpha^2 U(r). \quad (9)$$

Here α is the fine-structure constant, j takes on the values of either l or $-l-1$, where l is the orbital angular momentum of a particular partial wave, and the primes indicate radial derivatives. As in DW-1, the final-state distorting potential ($U=U_f$) is used for calculating both the initial-state and the final-state distorted waves [28]. For the static-exchange potential V_{ex}, the local approximation of Furness and McCarthy (1973) is used.

The final distinction between DW-1 and DW-2 lies in the fact that DW-2 has not been unitarized. It is well known that distorted-wave approximations without unitarization often exhibit a steep nonphysical increase in the integrated cross sections near threshold. Hence, the DW-2 results are not expected to be accurate for low energies (less than about 20-eV incident energy for the present case of interest).

In summary,

(1) DW-1 uses a semirelativistic method to calculate bound-state wave functions optimized for each final state while DW-2 uses the same bound-state wave functions as the BPRM-15 calculation;

(2) DW-1 does not include relativistic effects in the calculation of the distorted waves while DW-2 does; and

(3) DW-1 unitarizes the S matrix while DW-2 does not.

C. BPRM method

Details of this approach have been given by Bartschat and Grum-Grzhimailo [22] and will not be repeated here. Very briefly, we performed R-matrix (close-coupling-type) calculations with a varying number of states (5, 15, or 51) included in the close-coupling expansion. In the 51-state case, to be labeled as BPRM-51 below, we included the 31 physical states with configurations $4p^6$, $4p^5 5s$, $4p^5 5p$, $4p^5 4d$, and $4p^5 6s$, as well as 20 pseudostates with configurations $4p^5\overline{6p}$ and $4p^5\overline{7p}$, respectively. The principal reason for including the latter states was the fact that the $\overline{6p}$ and $\overline{7p}$ pseudoorbitals were constructed to improve the target description by effectively allowing for some term dependence in the bound orbitals, as well as to improve the wave function of the ground state. In the simpler calculations, only states with the configurations $4p^6$ and $4p^5 5s$ (BPRM-5) plus $4p^5 5p$ (BPRM-15) were coupled. Finally, relativistic effects were accounted for by including the one-electron terms of the Breit-Pauli Hamiltonian in the diagonalization of both the N-electron target and the $(N+1)$-electron collision problem.

III. RESULTS

It is well known that the success of obtaining reliable cross sections lies on an accurate description of the target. One way to compare the bound wave functions used in this work is the examination of the mixing coefficients, which are obtained by diagonalizing the Hamiltonian with level-specific Coulomb and spin-orbit parameters for each total angular momentum J. These mixing coefficients are listed in Table I, where each level is expressed in terms of the dominant LS designations. We list only the expansion coefficients of the 14 levels belonging to the $4p^5 5s$ and $4p^5 5p$ manifolds. Note that we have chosen to present the results in the $(LS)J$ rather than in the $(SL)J$ phase convention. Hence, there are some sign changes with respect to the coefficients given by Bartschat and Grum-Grzhimailo [22], but the only important aspect is, of course, a consistent treatment in either one of these phase conventions.

The close agreement between the expansion coefficients in the description of these levels obtained using single-configuration (DW-1) and close-coupling (BPRM) methods gives some confidence regarding the accuracy of the target descriptions. However, there is one important comment that needs to be made regarding the $(4p^6)$ admixture in the description of the excited $J=0$ states $2p_5$ and $2p_1$, respectively. Clearly, configuration interaction between the dominant $4p^5 5p$ configuration of the excited $2p$ states and the dominant $4p^6$ configuration of the ground state is, in principle, possible for the $J=0$ states. As will be shown below, theoretical results for excitation of the $2p_5$ and $2p_1$ states depend very strongly on that particular mixing coefficient. At this time, we only point out that this admixture is omitted in the DW-1 single-configuration model, while it is substantial in the BPRM-15 structure description. In the BPRM-51 model, however, the $4p^5\overline{6p}$ configuration, involving the $\overline{6p}$ pseudo-orbital, effectively accounts for electron correlations in the ground state and hence takes over the role played previously by the $4p^6$ admixture.

A. Excitation to the $4p^5 5s$ levels

In this section we compare and contrast our cross sections to the four levels in the $1s$ manifold. As can be seen from Table I, the $J=1$ levels $1s_4$ and $1s_2$ are heavily mixed while the metastable states $1s_5$ and $1s_3$ are purely LS coupled. The cross sections for excitations of these levels are shown in Fig. 2. (Due to the large number of coupled channels, the 51-state calculation could only be performed for energies up to 40 eV.) The minimal-coupling five-state BPRM calculation, which couples only the ground state and these four levels, is expected to yield the best agreement with the DW results, which contain no coupling, provided the same target description is used. As expected, the DW-2 results at higher energies are indeed in excellent agreement with the five-state BPRM cross sections for all the $1s$ transitions while the

TABLE I. *LSJ* mixing coefficients for the levels of the $4p^5 5s$ and $4p^5 5p$ configurations.

Level	Paschen notation	E (eV)[a]	DW-1	BPRM-15	BPRM-51[b]
$5s[\frac{3}{2}]^o_2$	$1s_5$	9.915	$1.0000\ ^3P$	$1.0000\ ^3P$	$0.99595s\ ^3P + 0.0735\ \ 4d\ ^3P + 0.0513\ \ \overline{6s}\ ^3P$
$5s[\frac{3}{2}]^o_1$	$1s_4$	10.033	$0.7363\ ^3P + 0.6766\ ^1P$	$0.6933\ ^3P + 0.7206\ ^1P$	$0.70625s\ ^1P + 0.7045\ \ 5s\ ^3P + 0.0588\ \ 4d\ ^3P$
$5s'[\frac{1}{2}]^o_0$	$1s_3$	10.563	$1.0000\ ^3P$	$1.0000\ ^3P$	$0.99155s\ ^3P + 0.1188\ \ 4d\ ^3P + 0.0522\ \ \overline{6s}\ ^3P$
$5s'[\frac{1}{2}]^o_1$	$1s_2$	10.644	$0.7363\ ^1P - 0.6766\ ^3P$	$0.6933\ ^1P - 0.7206\ ^3P$	$0.70685s\ ^1P - 0.7001\ \ 5s\ ^3P - 0.0866\ \ 4d\ ^3P$
$5p[\frac{1}{2}]_1$	$2p_{10}$	11.304	$0.9075\ ^3S - 0.3600\ ^3P + 0.2157\ ^1P + 0.0164\ ^3D$	$0.9129\ ^3S - 0.3505\ ^3P + 0.2086\ ^1P + 0.0154\ ^3D$	$0.9158\ \ 5p\ ^3S - 0.3455\ \ 5p\ ^3P + 0.1960\ \ 5p\ ^1P - 0.0565\ \ \overline{6p}\ ^3S$
$5p[\frac{5}{2}]_3$	$2p_9$	11.443	$1.0000\ ^3D$	$1.0000\ ^3D$	$0.9999\ \ 5p\ ^3D$
$5p[\frac{5}{2}]_2$	$2p_8$	11.445	$0.7123\ ^3D + 0.6833\ ^1D - 0.1602\ ^3P$	$0.7154\ ^3D + 0.6800\ ^1D - 0.1604\ ^3P$	$0.7198\ \ 5p\ ^3D + 0.6745\ \ 5p\ ^1D - 0.1664\ \ 5p\ ^3P$
$5p[\frac{3}{2}]_1$	$2p_7$	11.526	$0.7224\ ^1P + 0.4957\ ^3P - 0.4808\ ^3D + 0.0336\ ^3S$	$0.7184\ ^1P + 0.4942\ ^3P - 0.4883\ ^3D + 0.0338\ ^3S$	$0.7186\ \ 5p\ ^1P - 0.4906\ \ 5p\ ^3D + 0.4910\ \ 5p\ ^3P$
$5p[\frac{3}{2}]_2$	$2p_6$	11.546	$0.8700\ ^3P + 0.4386\ ^1D - 0.2252\ ^3D$	$0.8669\ ^3P + 0.4436\ ^1D - 0.2273\ ^3D$	$0.8643\ \ 5p\ ^3P + 0.4535\ \ 5p\ ^1D - 0.2173\ \ 5p\ ^3D$
$5p[\frac{1}{2}]_0$	$2p_5$	11.666	$0.7086\ ^3P - 0.7056\ ^1S$	$0.8039\ ^3P - 0.5893\ ^1S - 0.0803\ \ (4p^6)\ ^1S$	$-0.7281\ \ 5p\ ^1S + 0.6761\ \ 5p\ ^3P - 0.0936\ \ \overline{6p}\ ^1S$
$5p'[\frac{3}{2}]_1$	$2p_4$	12.101	$0.8693\ ^3D + 0.4570\ ^1P + 0.1807\ ^3P - 0.0526\ ^3S$	$0.8658\ ^3D + 0.4612\ ^1P + 0.1883\ ^3P - 0.0477\ ^3S$	$0.8601\ \ 5p\ ^3D + 0.4795\ \ 5p\ ^1P + 0.1629\ \ 5p\ ^3P - 0.0539\ \ 5p\ ^3S$
$5p'[\frac{1}{2}]_1$	$2p_3$	12.141	$0.7694\ ^3P - 0.4719\ ^1P + 0.4153\ ^3S + 0.1132\ ^3D$	$0.7729\ ^3P - 0.4771\ ^1P + 0.4040\ ^3S + 0.1083\ ^3D$	$0.7829\ \ 5p\ ^3P - 0.4639\ \ 5p\ ^1P + 0.3904\ \ 5p\ ^3S + 0.1369\ \ 5p\ ^3D$
$5p'[\frac{3}{2}]_2$	$2p_2$	12.144	$0.6648\ ^3D - 0.5836\ ^1D + 0.4663\ ^3P$	$0.6607\ ^3D - 0.5837\ ^1D + 0.4720\ ^3P$	$0.6590\ \ 5p\ ^3D - 0.5850\ \ 5p\ ^1D + 0.4732\ \ 5p\ ^3P$
$5p'[\frac{1}{2}]_0$	$2p_1$	12.257	$0.7086^1S + 0.7056^3P$	$0.7993\ ^1S + 0.5947\ ^3P + 0.0866\ \ (4p^6)\ ^1S$	$0.7366\ \ 5p\ ^3P + 0.6700\ \ 5p\ ^1S + 0.0819\ \ \overline{6p}\ ^1S$

[a]Reference [24].

[b]Mixing coefficients smaller than 0.05 are not given for BPRM-51.

DW-1 cross sections for the $1s_4$ level are closest to the 15-state BPRM predictions. The cross sections for the optically forbidden $1s_5$ and $1s_3$ metastable levels fall-off rapidly with increasing energy while the cross sections for the optically allowed $1s_4$ and $1s_2$ levels are nearly flat at high energies in all calculations shown in the figure. Due to the nonunitarity of the approach, the DW-2 cross sections exhibit a nonphysical steep increase with decreasing energy, particularly for the metastable $1s_5$ and $1s_3$ states.

None of the theories yields good agreement with the limited experimental data available for comparison [9,29], but we also note substantial discrepancies between the different experimental data sets. The large differences between the 51-state calculation and the 15-state calculation indicate the significant difficulty in obtaining convergence for these transitions. Note, however, that this difficulty is not simply due to a channel-coupling effect (otherwise the agreement between the five-state results and the DW-2 predictions would be most fortuitous), but has its origin at least partly in the changing target descriptions when more states are included and the optimization criteria are changed. For the $1s_4$ and $1s_2$ states, the DW-2 results are very similar to those from the five-state *R*-matrix calculation down to about 15 eV, and they are also in reasonable agreement with the data. For the metastable states, the DW-1 is in reasonable agreement with the data for the $1s_5$ state, but the agreement is worse for excitation of the $1s_3$ state. The BPRM-51 model, whose 15-eV results lie between the two sets of experimental data [9,16], is in accordance with both measurements up to factor of 2 for all four transitions over the entire energy range. As mentioned above, the large differences between the three *R*-matrix results and the two DW predictions demonstrates the strong dependence of the cross sections on the atomic wave functions. In fact, it can be argued that the quality of the target structure is in our case potentially more important than the theoretical method used to describe the collision processes, particularly for optically allowed transitions.

B. Excitation to the $4p^5 5p$ levels

In Figs. 3 and 4 we present our cross sections for excitation to the ten levels in the $2p$ manifold of the $4p^5 5p$ configuration from the ground state $4p^6\ ^1S_0$. Our cross sections from different theoretical predictions for the $2p_{10}$ through $2p_1$ levels are compared with the experimental data of Chilton *et al.* [16] and relativistic distorted-wave (RDW) calculations of Kaur *et al.* [12]. The peak values of the cross-sections measured by Bogdanova and Yurgenson [15] are not shown, because the authors did not give the corresponding electron energies. We present cross sections calculated by Kaur *et al.* [12] using both the single-configuration ground-state (RDW-*a*) and the multiconfiguration ground-state wave

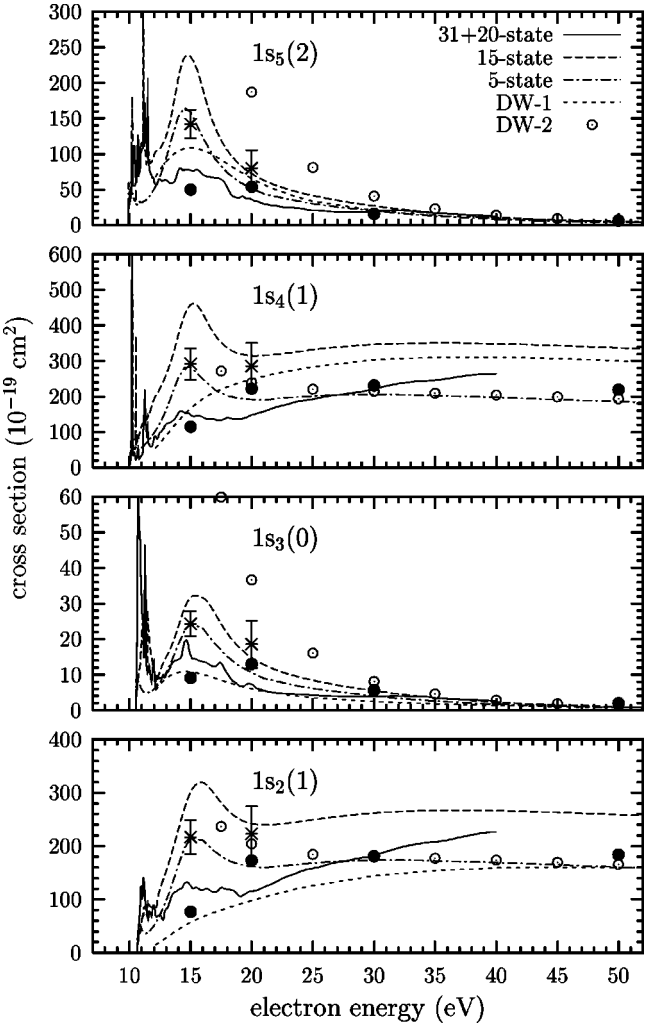

FIG. 2. Excitation cross sections from the ground state to the $1s_5$-$1s_2$ excited levels of the $4p^5 5s$ configuration as a function of collision energy. The J values of the final states are given in parentheses. The solid lines represent the 51-state BPRM calculation; long-dashed lines, 15-state BPRM results; dash-dotted lines, five-state BPRM results; short-dashed lines, DW-1 results; open circles, DW-2 results. The experimental data are from Trajmar *et al.* (●) [9] and Guo *et al.* (*) [29].

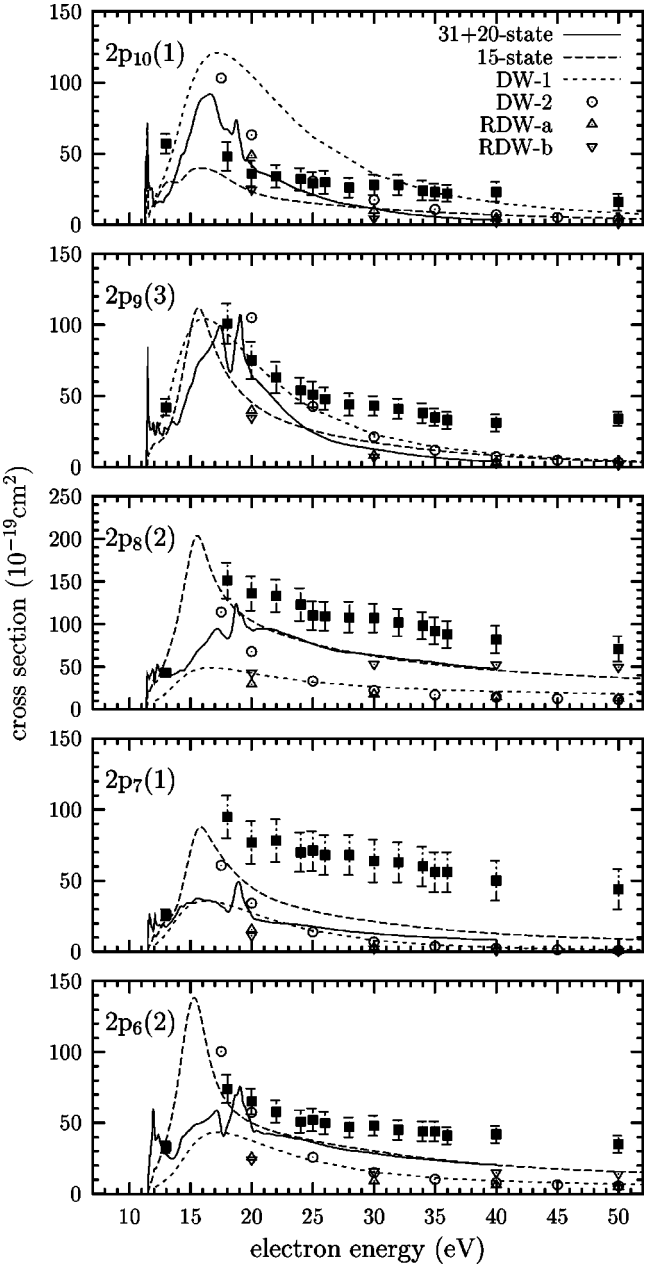

FIG. 3. Excitation cross sections from the ground state to the $2p_{10}$-$2p_6$ excited levels of the $4p^5 5p$ configuration as a function of collision energy. The J values of the final states are given in parentheses. The solid lines represent the 51-state BPRM calculation; long-dashed lines, 15-state BPRM results; short-dashed lines, DW-1 results; open circles, DW-2 results; triangles and inverted triangles, RDW-*a* and RDW-*b* calculations, respectively [12]; solid squares, experiment [16].

function (RDW-*b*). However, the RDW results of Ref. [12] are given only for energies above 20 eV, so we cannot make a comparison for energies near excitation thresholds. We note that Trajmar *et al.* [9] also presented integral cross sections to the levels in the $2p$ manifold; of these ten levels, however, they lumped some together and only kept the $2p_{10}$ and $2p_5$ levels isolated.

Among all the levels in the $2p$ manifold, the $2p_9$ ($J=3$) is the only purely LS-coupled state. All the theoretical cross sections of our study for this level agree reasonably well with each other for higher energies. The DW-1 and DW-2 cross sections are in close agreement down to an incident energy of about 20 eV below which nonunitarity causes DW-2 to become too large. For the low energies, DW-1 and BPRM-51 are in good agreement with the experimental data [16] for the $2p_9$ transition. For higher energies the theories are in good accord with each other and fall off with the expected E^{-3} behavior, whereas the experimental data [16] do not exhibit this energy dependence. The peak value of the cross section measured in [15] is at least a factor of 2 lower than in [16]; according to the data at 100 eV and 200 eV, the former, too, do not seem to decrease as fast with increasing energy as predicted in the calculations.

The $J=1$ excitations include the $2p_{10}$ and $2p_7$ levels in Fig. 3 and the $2p_4$ and $2p_3$ levels in Fig. 4. The DW-1 cross

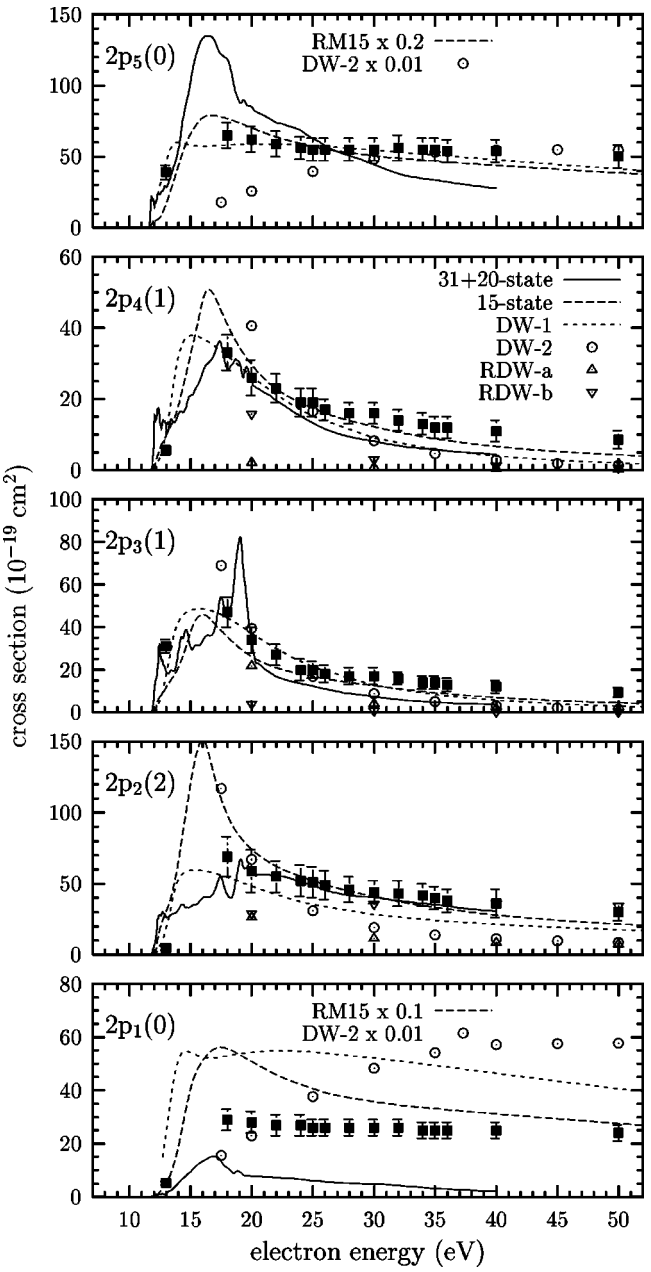

FIG. 4. Excitation cross sections from the ground state to the $2p_5$-$2p_1$ excited levels of the $4p^5 5p$ configuration as a function of collision energy. The J values of the final states are given in parentheses. The solid lines represent the 51-state BPRM calculation; long-dashed lines, 15-state BPRM results; short-dashed lines, DW-1 results; open circles, DW-2 results; triangles and inverted triangles, RDW-*a* and RDW-*b* calculations respectively [12]; solid squares, experiment [16].

sections for the $2p_{10}$ excitation in Fig. 3 are larger than the other predictions and closer to the experimental data for higher energies. All the other theories are in reasonably good agreement with each other for energies above 20 eV and all the theoretical results fall off faster than the experimental data at higher energies for $2p_{10}$. The cross sections presented by Trajmar *et al.* [9] for this level are generally much smaller than the measurements reported by Chilton *et al.* For the sake of clarity, the former are not shown in the figure.

The general trend for the other $J=1$ transitions ($2p_7$, $2p_4$, and $2p_3$) is similar, except that now the DW-1 results are closer to the other theories for intermediate and higher energies. For all $J=1$ cases, the present theories are in reasonable agreement with each other for higher energies, the theories fall off faster than the experimental data of Chilton *et al.* [16], and the BPRM and DW-1 results are in qualitative agreement with the experimental data near threshold. The large difference between experiment [16] and theory for the $2p_7$ state is striking. Note that the $2p_7$ state is one of the levels with highest indirect population [15,16]. The peak value of the cross section of $(24\pm 8)10^{-19}$ cm^2 for this level measured by Bogdanova and Yurgenson [15] is in good agreement with our BPRM-51 and DW-1 models. The cross sections of Chilton *et al.* [16] are closer to the value of 126 $\times 10^{-19}$ cm^2 given by Feltsan and Zapesochnyi [14], who ignored the cascade transitions. For the other $J=1$ transitions reported in [15], the peak cross section of $(24\pm 8)10^{-19}$ cm^2 for the $2p_4$ level is in satisfactory agreement with our 51-state BPRM and DW-1 calculations, as well as with the measurements [16], while the value of $(18\pm 6)10^{-19}$ cm^2 for the $2p_3$ level is lower than both our calculations and the measurements of [16]. For the four $J=1$ cases, experiment [16] and theory are closest at higher energies for $2p_4$ and $2p_3$. In general, the RDW results of Kaur *et al.* [12] tend to be somewhat smaller than the present results for these transitions and, therefore, are even further away from the experimental data of Chilton *et al.* [16]. The high-energy behavior of the measured cross sections of Chilton *et al.* is not well understood, but a similar behavior for excitation cross sections of the $J=1$ states has been noticed before in Ar I [4,7,12,30].

The cross sections for $J=2$ excitations to the $2p_8$ and $2p_6$ levels are shown in Fig. 3 and to the $2p_2$ level in Fig. 4. For the $2p_6$ and $2p_8$ levels, the cross sections of the DW-1 and DW-2 calculations are in excellent agreement by 25 eV, while both the 15-state and 51-state BPRM results are somewhat larger. The experimental data of Chilton *et al.* are again larger than all theoretical predictions except near threshold. For $2p_8$, the RDW-*a* results of Kaur *et al.* are in close agreement with the DW calculations, while the RDW-*b* predictions are close to the BPRM results at high energies. For $2p_6$, both the RDW calculations are close to the present DW calculations for higher energies. The 15-state BPRM cross sections have large, well-defined peaks in both of these transitions. The results for the remaining $J=2$ state $2p_2$ in Fig. 4 behave similarly to those for the $2p_8$ state in that the RDW-b results are closer to the BPRM and the RDW-a are lower and closer to the DW-2 results for higher energies. The primary difference for this transition is the fact that the DW-1 results are larger at high energies and somewhat closer to the BPRM results. Also, this is one of the few cases where the BPRM results are actually in good agreement with the experimental data over the entire energy range. The optical data of Bogdanova and Yurgenson [15] for the peak cross sections are $(81\pm 28)10^{-19}$ cm^2, $(17\pm 6)10^{-19}$ cm^2, and $(55\pm 8)10^{-19}$ cm^2 for the $2p_8$, $2p_6$, and $2p_2$ levels, respectively. This is in very good agreement with our 51-state

BPRM calculations for the $2p_8$ and $2p_2$ levels, and much lower for the $2p_6$ state in comparison with our calculations and the measurements of Chilton *et al.* [16].

The cross sections for the two forbidden $J=0$ monopole transitions to the $2p_5$ and $2p_1$ states are shown in Fig. 4. The peak cross sections from the two optical measurements [15,16] are in agreement for the $2p_1$ level, while the data of Bogdanova and Yurgenson [15] for the $2p_5$ level, $(31\pm 11)10^{-19}$ cm^2, are lower by approximately a factor of 2 than those of Chilton *et al.* [16]. Previous experience indicates that it is extremely difficult to predict accurate excitation cross sections for collisions involving monopole transitions, since the results are very sensitive to the target description. Although there is excellent agreement between experiment [16] and DW-1 for the $2p_5$ state, there is little similarity between experiment and the other theories. (Note that DW-2 and BPRM-15 are larger than experiment by factors of about 100 and 5–10, respectively.) Interestingly, the 51-state predictions lie *below* experiment by about a factor of 10.

Clearly, the monopole results are most unsettling. When predictions from two-different *R* matrix calculations differ by a factor of 100 and those from two-different distorted-wave calculations differ by two orders of magnitude as well, it is impossible to argue that either one represents a reliable model. Consequently, we performed further test calculations to gain a better understanding of these transitions. These calculations revealed that the $4p^6$ configuration played a key role in the monopole transitions. From Table I, it is seen that the $2p_5$ and $2p_1$ wave functions used in the DW-1 calculation do not have a $4p^6$ contribution while the BPRM-15 and, therefore, the DW-2 excited-state wave functions contain a significant admixture. Consequently, we decided to investigate the importance of this particular term.

As a first step, we tried to improve the description of the $J=0$ states used in the DW-2 calculations. To accomplish this, we used the program package SUPERSTRUCTURE of Eissner *et al.* [31] and optimized the bound orbitals on the particular final states of interest. As an example, this procedure produced the following $2p_2$ and $2p_1$ wave functions (which we label as SS15):

$$2p_2(\mathrm{SS15}) = 0.6367(4p^5 5p)^3D_2 - 0.6001(4p^5 5p)^1D_2 + 0.4842(4p^5 5p)^3P_2, \quad (10)$$

$$2p_1(\mathrm{SS15}) = 0.8978(4p^5 5p)^1S_0 + 0.4387(4p^5 5p)^3P_0 - 0.0391(4p^6)^1S_0. \quad (11)$$

Comparing the above coefficients with the corresponding BPRM-15 coefficients from Table I, we see a relatively small change in the $2p_2$ coefficients and a somewhat larger change in the $2p_1$ coefficients. The largest percentage change occurs in the $4p^6$ coefficient, which was reduced by more than a factor of 2 and even changed sign. Since it was clear that the strength of the $4p^6$ contribution was important, we also performed calculations using the BPRM-15 and SS15 wave functions with the $4p^6$ term eliminated (and the weights appropriately renormalized). The results of these test calculations are shown in Fig. 5 for excitation of the $2p_2$ $(J=2)$ and the $2p_1$ $(J=0)$ states.

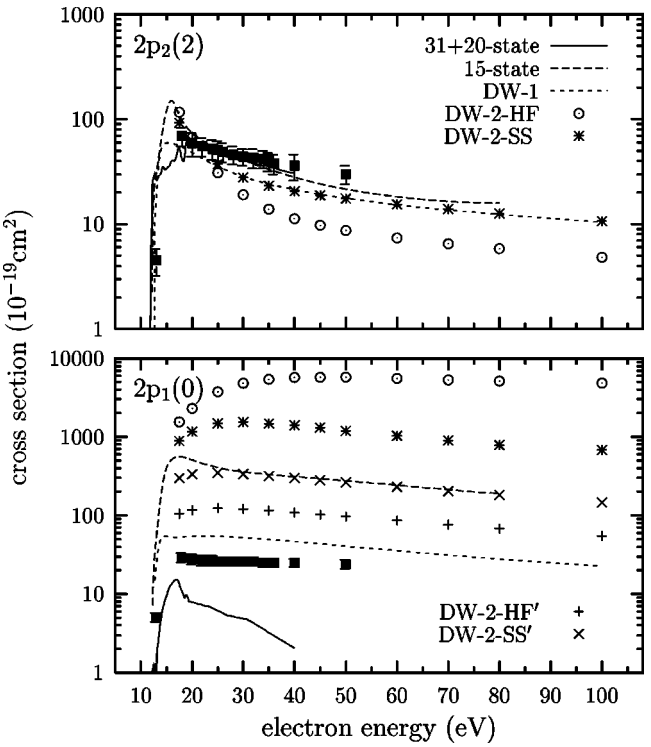

FIG. 5. Excitation cross sections from the ground state to the $2p_2$ and $2p_1$ excited levels of the $4p^5 5p$ configuration as a function of collision energy. The J values of the final states are given in parentheses. The solid lines represent the 51-state BPRM calculation; long-dashed lines, 15-state BPRM results; short-dashed lines, DW-1 results; ○, DW-2 results with the HF wave functions used in the BP15 calculation; *, DW-2 results with orbitals from SUPERSTRUCTURE [31]; +, DW-2 results with HF orbitals without the $4p^6$ contribution; ×, DW-2 results with SS orbitals without the $4p^6$ contribution; solid squares, experiment [16].

As mentioned above, the DW-1 results were higher than the DW-2 and closer to the BPRM results for excitation of the $2p_2$ state. The small change in coefficients obtained in the SS15 wave functions produced excellent agreement between DW-1 and DW-2 for excitation of the $2p_2$ state. For excitation of the $2p_1$ state, the various calculations still produced very-different results. Comparing DW-2 with DW-2 using the SS15 target description, it is seen that reducing the weight of the $4p^6$ term by a factor of 2, reduced the cross section by almost a factor of 10. Furthermore, it is seen that removing the $4p^6$ term completely from the DW-2 wave function reduced the cross section by a factor of about 200 while removing it from the SS15 wave function reduced the cross section by less than a factor of 10. By coincidence, the SS15 results without the $4p^6$ term are almost the same as the BPRM-15 results.

The above studies suggest that the good agreement with experiment for the $2p_5$ state, and the disagreement by ''only a factor of 2'' for the $2p_1$ state, found in the DW-1 calculation resulted from the omission of the $4p^6$ configuration in the description of these target states. It is clear that a proper

treatment of the $4p^6$ configuration is required for a satisfactory theoretical description of this problem.

IV. CONCLUSIONS

Using various distorted-wave and close-coupling methods, we have investigated electron-impact cross sections for excitation of Kr I from the ground state to the 14 excited states of the $4p^5 5s$ and $4p^5 5p$ configurations. As noted in [22], when the close-coupling expansions show reasonable convergence with the number of states included in the expansion, the results are generally in better agreement with experiment than those calculated with other methods. Nevertheless, since distorted wave-methods based on a first-order theory can very easily account for term-dependent target descriptions, they may be expected to give more-reliable results at higher energies when channel-coupling effects diminish relative to the structure problem. Thus, these two methods should be expected to complement each other. For an atom such as krypton with a nuclear charge $Z=36$, relativistic effects may also become important. Although our DW methods are not fully relativistic, the DW-1 method has included relativistic mass-velocity and Darwin terms in optimizing the orbitals and both DW methods include the spin-orbit interaction in diagonalizing the Hamiltonian to obtain mixing coefficients for the levels. Furthermore, the DW-2 method accounts for relativistic effects in the calculation of the continuum states.

The reasonably good agreement between the five-state BPRM calculations and the DW predictions for the levels in the $1s$ manifold is satisfying. The hope of a study such as this would be that the BPRM results yield good agreement with experiment for low energies, the DW results are valid for high energies, and the two theories converge together for intermediate energies, and thus one would have a reliable theory for all collision energies. This satisfying situation was indeed found for excitation of Ar I from excited metastable states [6]. Unfortunately, it was not found to be the case here, most likely due the large excitation energies and the different description of the inner-target electrons in the ground state and the excited states. The BPRM-51 results do not smoothly join with any of the DW theories with increasing energy, except for transitions with very-small cross sections. The lower-order BPRM-5 results smoothly join with the DW-2 results for excitation of the $1s$ states, but this is primarily of academic interest. The BPRM method is expected to be valid at low energies. For several of the transitions, the BPRM-51 results were indeed in reasonable accord with the experimental data, with notable exceptions being excitation to the $J=0$ $2p_5$ and $2p_1$ states. Nevertheless, for many levels the experimental data on the cross sections from three different measurements [9,15,16] do not agree with each other within the published uncertainties, and the calculations cannot confirm any one of them unambiguously.

For most of the transitions investigated in this work, the theoretical predictions are in better agreement with each other than with the experimental data, and the theoretical results for forbidden transitions generally decrease much faster with increasing collision energy than what it seen experimentally. The experimentally determined energy dependence of the cross sections is unexpected and currently unexplained. The most troublesome transitions are those involving the $J=0$ $2p_5$ and $2p_1$ levels. We have shown that the treatment of the $4p^6$ admixture is crucial for these levels and that large changes in the theoretical cross sections are produced by small changes in the weight of this particular term. From a practical point of view, it seems advisable to simply omit this configuration in the description of the excited-state wave function. However, this is a less than satisfactory remedy to the problem.

The need for accurate cross sections for electron-impact excitation of Kr I and the finding of considerable differences between theoretical predictions and experimental data suggest that much-more work, both in experiment and theory, is required before this collision problem is understood in a satisfactory way.

ACKNOWLEDGMENTS

The authors would like to acknowledge receiving additional data beyond those published from J. E. Chilton. This work was supported, in part, by BMDO, the Office of Naval Research (A.D.), the Foundation ''Universities of Russia; Basic Research'' under Grant No. 5340 (A.N.G), and the National Science Foundation under Grant Nos. PHY-0088917 (K.B.) and PHY-0070872 (D.V. and D.H.M.).

[1] G. G. Lister, in *Advanced Technologies Based on Wave and Beam Generated Plasmas*, edited by H. Schluter and A. Shivarova (Kluwer Academic Publishers, Boston, 1999), p. 65.

[2] M.V. Malyshev, V.M. Donnelly, and S. Samukawa, J. Appl. Phys. **84**, 1222 (1998).

[3] M.V. Malyshev and V.M. Donnelly, Phys. Rev. E **60**, 6016 (1999).

[4] D.H. Madison, C.M. Maloney, and J.B. Wang, J. Phys. B **31**, 873 (1998).

[5] K. Bartschat and V. Zeman, Phys. Rev. A **59**, R2552 (1999).

[6] C.M. Maloney, J.L. Peacher, K. Bartschat, and D.H. Madison, Phys. Rev. A **61**, 022701 (2000).

[7] A. Dasgupta, M. Blaha, and J.L. Giuliani, Phys. Rev. A **61**, 012703 (2000).

[8] G.D. Meneses, F.J. da Paixão, and N.T. Padial, Phys. Rev. A **32**, 156 (1985).

[9] S. Trajmar, S.K. Srivastava, H. Tanaka, H. Nishimura, and D.C. Cartwright, Phys. Rev. A **23**, 2167 (1981).

[10] I.I. Fabrikant, O.B. Shpenik, A.V. Snegursky, and A.N. Zavilopulo, Phys. Rep. **159**, 1 (1988).

[11] S.J. Buckman and C.W. Clark, Rev. Mod. Phys. **66**, 539 (1994).

[12] S. Kaur, R. Srivastava, R.P. McEachran, and A.D. Stauffer, J. Phys. B **31**, 4833 (1998).

[13] I.P. Zapesochnyi and P.V. Feltsan, Opt. Spektrosk. **20**, 521 (1966) [Opt. Spektrosk. **20**, 291 (1966)].
[14] P.V. Feltsan and I.P. Zapesochnyi, Ukr. Fiz. Zh. (Russ. Ed.) **12**, 1452 (1967) [Ukr. Fiz. Zh. (Russ. Ed.) **12**, 1376 (1967)].
[15] I.P. Bogdanova and S.V. Yurgenson, Opt. Spektrosk. **62**, 713 (1987) [Opt. Spektrosk. **62**, 424 (1987)].
[16] J.E. Chilton, M.D. Stewart, Jr., and C.C. Lin, Phys. Rev. A **62**, 032714 (2000).
[17] D.H. Madison and W.N. Shelton, Phys. Rev. A **7**, 499 (1973).
[18] K. Bartschat and D.H. Madison, J. Phys. B **20**, 5839 (1987).
[19] K.A. Berrington, W.B. Eissner, and P.H. Norrington, Comput. Phys. Commun. **92**, 290 (1995).
[20] V. Zeman and K. Bartschat, J. Phys. B **30**, 4609 (1997).
[21] V. Zeman, K. Bartschat, T.J. Gay, and K.W. Trantham, Phys. Rev. Lett. **79**, 1825 (1997).
[22] K. Bartschat and A.N. Grum-Grzhimailo, J. Phys. B **33**, 4603 (2000).
[23] V. Zeman, K. Bartschat, C. Norén, and J.W. McConkey, Phys. Rev. A **58**, 1275 (1998).
[24] C. E. Moore, *Atomic Energy Levels*, NSRDS-NBS 35 (U.S. GPO, Washington, DC, 1971).
[25] J.K. O'Connell and N.F. Lane, Phys. Rev. A **27**, 1893 (1983).
[26] A. Jain, B. Etemadi, and K.R. Karim, Phys. Scr. **41**, 321 (1989).
[27] E. Clementi and C. Roetti, At. Data Nucl. Data Tables **14**, 177 (1974).
[28] D.H. Madison, J. Phys. B **12**, 3399 (1979).
[29] X. Guo, D.F. Mathews, G. Mikaelian, M.A. Khakoo, A. Crowe, I. Kanik, S. Trajmar, V. Zeman, K. Bartschat, and C.J. Fontes, J. Phys. B **33**, 1895 (2000).
[30] V.E. Bubelev and A.N. Grum-Grzhimailo, J. Phys. B **24**, 2183 (1991).
[31] W. Eissner, M. Jones, and H. Nussbaumer, Comput. Phys. Commun. **8**, 270 (1974).